Supramolecular structural changes of waxy and high-amylose cornstarches heated in abundant water

ARTICLE *in* FOOD HYDROCOLLOIDS · MARCH 2014

Impact Factor: 4.09 · DOI: 10.1016/j.foodhyd.2013.08.028

6 AUTHORS, INCLUDING:

Xiaoxi Li
South China University of Technology
39 PUBLICATIONS **465** CITATIONS

SEE PROFILE

David Fengwei Xie
University of Queensland
58 PUBLICATIONS **1,114** CITATIONS

SEE PROFILE

Food Hydrocolloids 35 (2014) 700–709

Contents lists available at ScienceDirect

Food Hydrocolloids

journal homepage: www.elsevier.com/locate/foodhyd

Supramolecular structural changes of waxy and high-amylose cornstarches heated in abundant water

Binjia Zhang [a], Yue Zhao [a], Xiaoxi Li [a], Lin Li [a], Fengwei Xie [b], Ling Chen [a, *]

[a] Ministry of Education Engineering Research Center of Starch & Protein Processing, Guangdong Province Key Laboratory for Green Processing of Natural Products and Product Safety, College of Light Industry and Food Sciences, South China University of Technology, Guangzhou 510640, China
[b] Australian Institute for Bioengineering and Nanotechnology, The University of Queensland, Brisbane, Qld 4072, Australia

ARTICLE INFO

Article history:
Received 7 May 2013
Accepted 27 August 2013

Keywords:
Cornstarch
Amylose/amylopectin ratios
Supramolecular structure
Hydrothermal treatment
Abundant water

ABSTRACT

Being heated in abundant water, native waxy cornstarch displayed only one endotherm (G), while there were two endotherms (G and M2) for native Gelose 50 (G50) cornstarch. Waxy cornstarch granules could swell dramatically at around the T_o of endotherm G, while G50 cornstarch granules presented a less significant increase in the volume near the T_o of endotherm G. As the temperature increased up to 70 °C, the scattering objects in both of the cornstarches became looser. Interestingly, when the temperature was 75 °C or higher, mass fractal structures at three scale levels emerged for waxy cornstarch, and a mass fractal structure at the higher scale level and a surface fractal structure at the lower scale level appeared for G50 cornstarch, suggesting the inhomogeneity at a nano-colloidal level and a nano-particle level respectively for the two starches. The scattering objects at the lower or intermediate scale level could form a mass fractal structure at the higher scale level with different compactness (D_{m1}). The average thickness of the semi-crystalline lamellae (d) of the both cornstarches changed slightly with an increase in the temperature and finally disappeared due to the multiple fractal structures. Additionally, the A-type crystalline structure of waxy cornstarch and the B-type crystalline structure of G50 cornstarch displayed a similar trend with the temperature regarding the anisotropy. For G50 cornstarch, the V-type crystalline structure required a higher temperature to complete its melting.

1. Introduction

Starch is traditionally the main material for foods and is one of the most important energy sources for humans (Juansang, Puttanlek, Rungsardthong, Puncha-arnon, & Uttapap, 2012). Due to its total biodegradability, low cost, worldwide availability from a large number of crops, and potential health benefits, starch has gained attention as a polymer resource for eco-friendly and nutritional uses (Bastos, Santos, da Silva, & Simao, 2009). Normally, it consists of 10–30% amylose, a mostly linear 1,4-α-D-glucan with a small number of long branches, and 90–70% amylopectin, mainly 1,4-α-D-glucan but having a large number of 1,6-α linkages at the branch points (Jiang, Gao, Li, & Zhang, 2011; Karim, Norziah, & Seow, 2000; Zobel, 1988). While high-amylose starch can possess the amylose content up to 85%, waxy starch may contain 100% amylopectin (Liu, Halley, & Gilbert, 2010). The structure of native starch is organized in four length scales, i.e., the whole granular morphology (μm), the growth rings (~0.1 μm), the lamellar structure (8–9 nm), and the molecular scale (~0.1 nm) (Pikus, 2005).

Amylose and amylopectin molecules can form amorphous and crystalline regions in the starch granule (Oates, 1997), which is the basis of the supramolecular structure (the granular morphology, the fractal structure, the lamellar structure, and the crystalline structure) of starch. It is shown that two kinds of fractal structures, the mass fractal form and the surface fractal form, have been found using the small-angle X-ray scattering (SAXS) technique (Zhang, Chen, Zhao, & Li, 2013; Zhang, Li, Liu, Xie, & Chen, 2013). Moreover, there are two main types of crystalline structures of starch (Kim & Huber, 2010; Nara & Komiya, 1983), i.e. the A-type crystalline structure of cereal starches such as wheat and rice starches, and the B-type crystalline structure of tuber, fruit and stem starches such as potato and banana starches; additionally, the C-type crystalline structure, which is actually a combination of both the A- and B-type structures (Gernat, Tadosta, & Damaschun, 1990; Sarko & Wu, 1978), and the V-type crystalline structure, describing the amylose single-helices co-crystallized with compounds such as iodine, dimethyl sulfoxide (DMSO), alcohols, or fatty acids, were

* Corresponding author. Tel./fax: +86 20 8711 3252.
E-mail addresses: felchen@scut.edu.cn, zbw9383@163.com (L. Chen).

0268-005X/$ – see front matter © 2013 Elsevier Ltd. All rights reserved.
http://dx.doi.org/10.1016/j.foodhyd.2013.08.028

also detected by the X-ray diffraction (XRD) technique (Buleon, Colonna, Planchot, & Ball, 1998).

With hydrothermal treatment in abundant water which is one of the key processes for starchy products in food industry, the supramolecular structure of starch may be influenced. Particularly, if the temperature is higher than a specific value, starch granules undergo an irreversible swelling and the crystalline structure of starch is destroyed; the gelatinization of starch can thus be completed (Atwell, Hood, Lineback, Varriano-Marston, & Zobel, 1988). It is widely accepted that the gelatinization of starch is comprised of three stages: (i) a small amount of moisture is absorbed into the starch granule without affecting the crystalline structure and the basic characteristics; if dehydrated, the starch granule can restore to its original state. This is the reversible bibulous stage. (ii) In the subsequent irreversible bibulous stage, with an increase in the temperature, water gradually enters into the crystalline regions, making the hydrogen bonds in starch molecules become unstable and break down; thus, the crystalline organization changes into amorphous regions. In this stage, the starch granule rapidly becomes 50–100 times bigger in its volume, and cannot recover to the initial structure. (iii) In the final stage, with even higher temperature, all starch granules are destroyed to form a gel (Zhang, Chen, et al., 2013; Zhang, Li, et al., 2013). Therefore, hydrothermal treatment in abundant water can lead to changes in the crystalline structure, and other supramolecular characteristics, of starch. It is worth noting that the supramolecular structures of starch play a key role in determining the properties (Kim & Huber, 2010). Particularly, the fractal structure and the crystalline structure (Zhang, Chen, et al., 2013; Zhang, Li, et al., 2013) have an influence on the enzymatic resistivity of starch (resistant starch content) which displays a nutritional relevance and potential health benefits. However, studies on the detailed supramolecular structural changes of waxy and high-amylose cornstarches heated in abundant water are limited, which is undesirable for further investigation on the detailed relationships between the supramolecular structures and properties of starch.

In this study, the thermal behaviors of native waxy and Gelose 50 (G50) cornstarches, as well as the related detailed changes in the granular morphology, fractal characteristics, lamellar structure, mixing within phases, scattering invariant, and crystalline structure, as heated in abundant water, were investigated. The results of this study provide new information on the changes in the supramolecular structures at different scale levels of waxy and high-amylose cornstarches by hydrothermal treatment in abundant water.

2. Material and methods

2.1. Materials

Cornstarches with different amylose/amylopectin ratios (Waxy, 1/99; G50, 50/50) were used in the experimental work. All the starches were commercially available and kindly supplied by Penford (Australia). The moisture content (MC) of each sample was determined using a moisture analyzer (MA35, Sartorius Stedim Biotech GmbH, Germany). The lipid content was determined using the method described by Chang et al. (Chang, He, & Huang, 2013). The total lipid, free lipid, and bound lipid contents of waxy cornstarch were 0.47, 0.42 and 0.05 (g/100 g dry starch) respectively, while the total lipid, free lipid, and bound lipid contents of G50 cornstarch were 1.26, 0.39 and 0.87 (g/100 g dry starch) respectively.

2.2. Sample preparation

About 50 mL of deionized water in a vial was heated to a certain temperature (45, 50, 55, 60, 65, 70, 75, 80, 85, and 90 °C) in a water bath, then 1 g of dry starch was added into the deionized water and incubated for 30 min with stirring. The samples were collected by filtering with a vacuum filter and 15 μm filter paper (Hangzhou Whatman-Xinhua Filter Paper Co., Ltd, China), freezed immediately using liquid nitrogen, and freeze dried at −40 °C for 48 h. Finally, all samples were grounded for further analysis. In the following discussion, codes typically as “Waxy-65” will be used, where “Waxy” means the type of cornstarch and “65” means the temperature the starch was heated at.

2.3. Differential scanning calorimetry (DSC)

The thermal characteristics of native waxy and G50 cornstarches were measured using a PerkinElmer DSC Diamond-I with an internal coolant (Intercooler 1P) and nitrogen purge gas. A high-pressure stainless steel pan (PerkinElmer No.: B0182901) with a gold-plated copper seal (PerkinElmer NO. 042-191758) was used to maintain a constant MC during the DSC measurements. The native cornstarch samples, with about 75% MC, were prepared by premixing the starches with added water in sealed glass vials, which were kept at 20 °C for 24 h before the measurement to achieve homogeneous samples. About 15 mg sample, scanned from 40 to 170 °C, was used in the study. The temperature lag due to the large mass of the stainless steel pan was minimized by using a slow heating rate of 5 °C/min. The onset temperature (T_o), peak temperature (T_p), conclusion temperature (T_c), and enthalpy (ΔH) of starch gelatinization were recorded. The enthalpy was calculated based on the weight of dry starch. All the results are reported as the averages of 3 replicates.

2.4. Microscopy

Ordinary/polarized light microscopy was performed using a polarized light microscope (PLM) (Axioskop 40 Pol/40A Pol, ZEISS, Oberkochen, Germany) equipped with a 35 mm SLA camera (Power Shot G5, Canon, Tokyo, Japan). The magnification was 500 (50 × 10). Each sample was dispersed as 10 mg of starch in 1 mL of distilled water in a glass vial. Then, a drop of the starch suspension was transferred onto a slide and covered by a cover slip. Ordinary and polarized light was used for observation.

2.5. Small-angle X-ray scattering (SAXS)

A SAXSess SAXS system (Anton Paar, Austria), operated at 50 mA and 40 kV, using Cu Kα radiation with a wavelength of 0.1542 nm as the X-ray source was applied to perform the SAXS measurements according to our previously method (Zhu, Li, Chen, & Li, 2012) with proper modification. Each sample was placed in a paste sample cell and was exposed at the incident X-ray monochromatic beam for 10 min. The data, recorded using an image plate, were collected by the IP Reader software with a PerkinElmer storage phosphor system. The samples used for the SAXS measurement were prepared by premixing the starch with added water in glass vials and were equilibrated at 20 °C for 24 h before the analysis. The total MC of each sample was 65%. All data were normalized, and the background intensity and smeared intensity were removed using SAXSquant 3.0 software for further analysis. The relationship between q and θ can be calculated by: $q = (4\pi \sin\theta)/\lambda$ (where λ (nm) is the wavelength of the X-ray source and q (nm^{-1}) is the scalar of scattering vector) (Suzuki, Chiha, & Yano, 1997).

2.6. Wide-angle X-ray diffraction (WAXD)

The data at the region of $5 < q < 25$ nm^{-1}, obtained in the SAXS measurements, were used as the WAXD results. The background

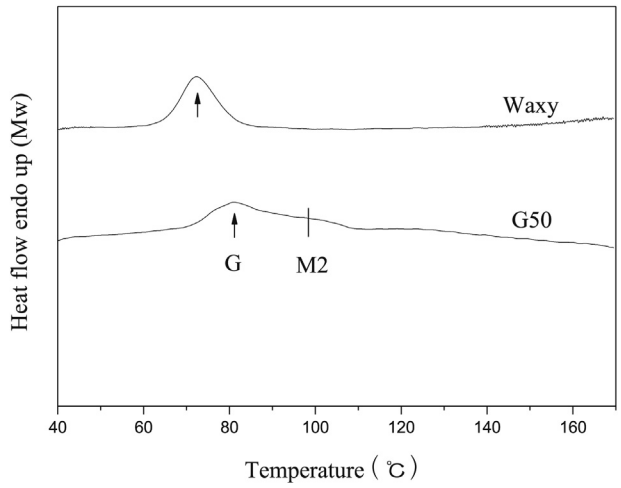

Fig. 1. DSC thermograms of native waxy and high-amylose cornstarches in abundant water.

scattering intensity was removed using the SAXSquant 3.0 software.

2.7. Attenuated total reflectance Fourier transform infrared spectroscopy (ATR-FTIR)

The ATR-FTIR spectra of the cornstarches were measured using a Tensor 37 spectrometer (Bruker, Germany) equipped with a deuterated triglycine sulfate (DTGS) detector. The spectra, recorded against an empty cell as the background, were acquired at wavelength between 800 and 1200 cm^{-1} with 4 cm^{-1} resolution with the OPUS software. All spectra were the averages of 64 scans and were baseline corrected and normalized. The absorbance intensities of the bands at about 1047 and 1022 cm^{-1} were used to investigate the crystalline structure. All the samples had the same MC.

3. Results and discussion

3.1. Thermal behaviors of native cornstarches

The thermal behaviors of a variety of starches have been measured by DSC (Liu, Yu, Xie, & Chen, 2006; Wang et al., 2011). Fig.1 Table 1 present the gelatinization behaviors of the native cornstarches with different amylose/amylopectin ratios in abundant water. It is seen that only one endotherm (G) was observed for native waxy cornstarch, attributed to the melting of amylopectin, while there were two endotherms (G and M2) for native G50 cornstarch, related to the melting of amylopectin and amylose–lipid complex respectively. This can be demonstrated by the fact that compared with native waxy cornstarch, native G50 cornstarch contained more amylose and most of its lipid was bounded (see 2.1). For the endotherm G, native G50 cornstarch displayed a higher T_o, T_p, T_c, and ΔT but smaller ΔH than native waxy cornstarch (see Table 1), indicating the requirement of a higher temperature for the gelatinization of the amylopectin of native G50 cornstarch. According to previous studies (Liu et al., 2006; Yu & Christie, 2001), the endotherm in DSC measurements depends on the cornstarch source, MC, the ratio of amylose/amylopectin, and the measurement conditions.

3.2. Changes in granular morphology

Fig. 2 shows the microscopic images under ordinary and polarized lights of cornstarches with different amylose/amylopectin ratios heated in abundant water at different temperatures. It can be observed that native waxy cornstarch displayed a mixture of rounded granules from the floury endosperm, and angular granules from the horny endosperm with four or five sides, while native G50 cornstarch consisted of rounded granules, angular granules, and small irregular pieces. Additionally, the granules of native waxy cornstarch were more regular in shape and larger than those of native G50 cornstarch. The granules of both kinds of starches swelled with the temperature increase. Particularly, a sharp increase in the size of granules was seen for Waxy-65, and then the granules became larger and even broken at a higher temperature (75 °C); however, G50 cornstarch did not display apparent swelling until the temperature reaching 75 °C, and an even higher temperature led to the swelling of more granules without a drastic increase in the volume. This suggests that being heated in excess water, waxy cornstarch granules could swell dramatically at around the T_o of endotherm G and even break at a temperature (75 °C) lower than the T_c of endotherm G, while the granules of G50 cornstarch presented a less significant increase in the volume at a temperature higher than the T_o of endotherm G and no granules disappeared during the melting of amylopectin. One explanation for this phenomenon could be that the amylose–lipid complex needed a higher temperature to complete its melting, thus the granules of G50 cornstarch were more difficult to swell and even to break during the hydrothermal treatment.

3.3. Fractal characteristics

According to previous reports (Suzuki et al., 1997; Zhang, Chen, et al., 2013; Zhang, Li, et al., 2013), the fractal characteristics of starch can be analyzed using the SAXS patterns. Moreover, the mass fractal dimension (D_m) is used to indicate the compactness, whereas the surface fractal dimension D_s is seen as an indicator of the degree of smoothness of the scattering objects, and the value of D_s is equal to 2 when the surface of the scattering objects is smooth (Suzuki et al., 1997). Additionally, the scattering objects of surface fractals are more compact than those of mass fractals, and the D_m which is slightly smaller than 1 can be used to describe the mass fractal scattering objects which are very loose. Fig. 3 a and b show the double-logarithmic SAXS patterns shifted along the ordinate of waxy and G50 cornstarches heated in abundant water, in which a straight-line segment at the low q region was seen for both of the native cornstarches, attributed to the existence of a fractal structure. As the results shown in Table 2, native waxy cornstarch possessed a mass fractal structure with $D_{m1} = 2.67$ in the range of around 39.50 nm $< d$ (2π/

Table 1
DSC parameters of native waxy and high-amylose cornstarches.

Sample	Endotherm G					Endotherm M2				
	T_o (°C)	T_p (°C)	T_c (°C)	ΔT (T_c–T_o)	ΔH (J/g)	T_o (°C)	T_p (°C)	T_c (°C)	ΔT (T_c–T_o)	ΔH (J/g)
Waxy	65.06	72.33	81.25	16.19	18.87	–	–	–	–	–
G50	71.07	81.08	92.54	21.47	14.90	85.05	96.26	107.34	22.29	4.56

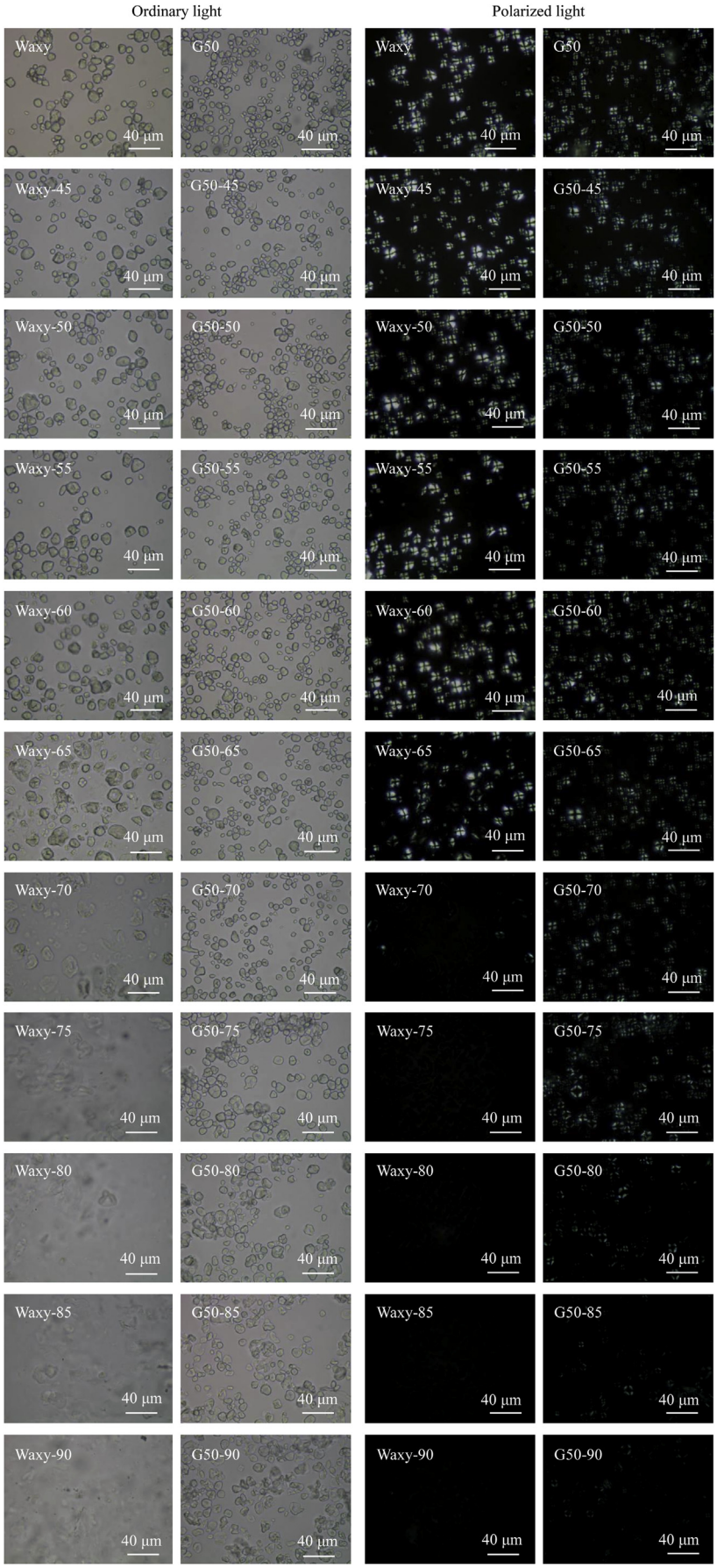

Fig. 2. Microscopic images of native and hydrothermally treated waxy and high-amylose cornstarches.

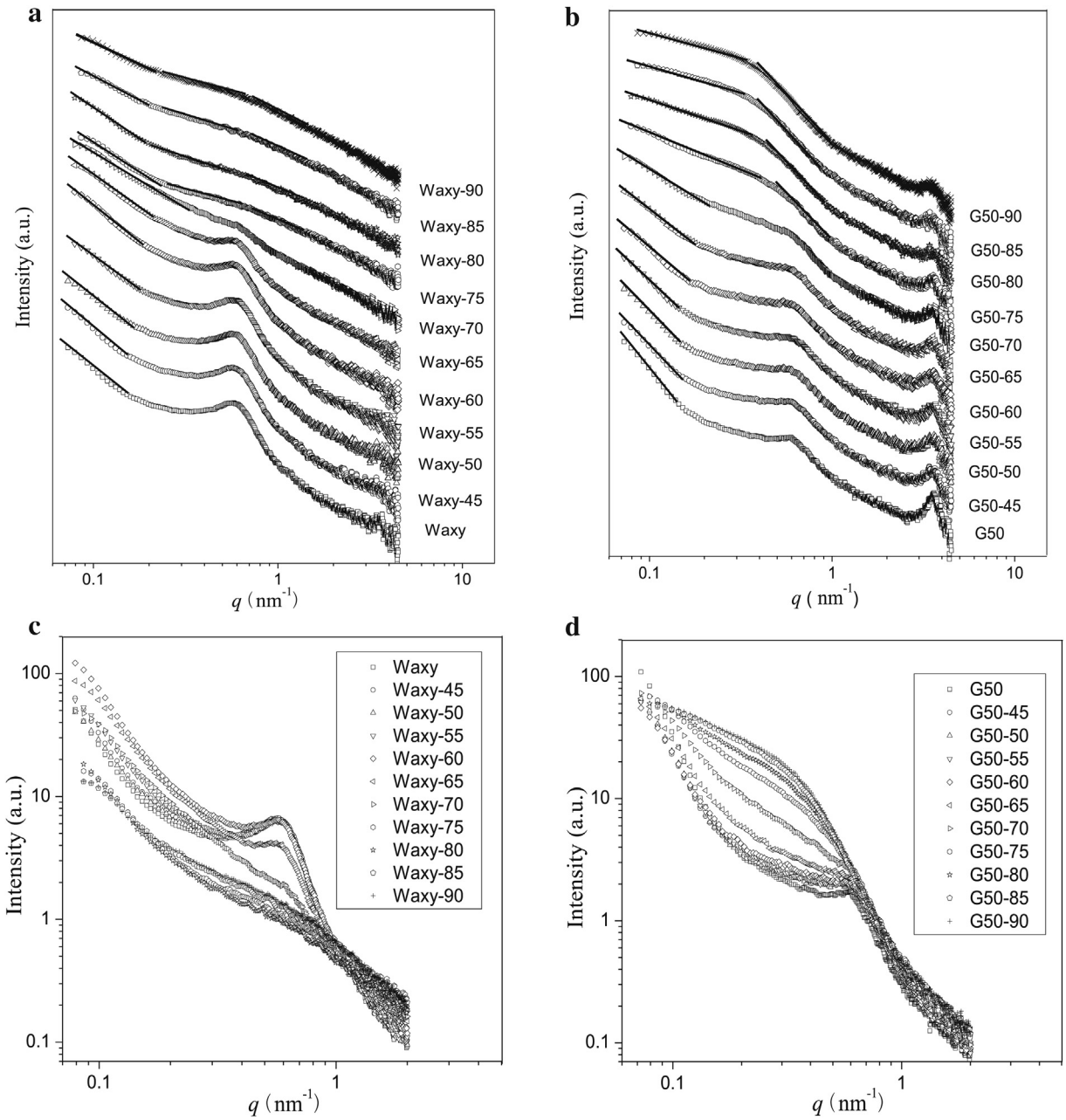

Fig. 3. Double-logarithmic SAXS patterns of native and hydrothermally treated waxy and high-amylose cornstarches (waxy (a, c), G50 (b, d)). The solid lines show the relationship $I \sim q^{-\alpha}$.

q) < 80.00 nm, whereas native G50 cornstarch displayed a surface fractal structure with $D_{s1} = 2.07$ at the same scale level, indicating the scattering objects in native G50 cornstarch were more compact and possessed a smooth surface. With the temperature increasing to 70 °C, the scattering objects in waxy cornstarch formed a mass fractal structure in a larger scale range with generally a decrease in D_{m1}, while the fractal structure of G50 cornstarch changed from surface fractals to mass fractals. This implies that the scattering objects in both waxy and G50 cornstarches became looser. To be more precise, when the temperature reached 70 °C, waxy cornstarch possessed a mass fractal structure, with $D_{m1} = 1.94$ in the range of around 23.79 nm < d < 80.00 nm, and G50 cornstarch also displayed a mass fractal structure, with $D_{m1} = 2.16$ in the range of around 38.06 nm < d < 80.00 nm.

Interestingly, with the temperature equal to or higher than 75 °C, the SAXS patterns of waxy cornstarch samples were characterized by three linear regions, whereas all the G50 cornstarch samples had a shoulder-like pattern at the q region of 0.2–0.4 nm^{-1}. This demonstrates the existence of fractal scattering regions at different q regions with different fractal dimensions as reported earlier (Zhang, Chen, et al., 2013; Zhang, Li, et al., 2013). Further, the three straight-line segments in the SAXS patterns of waxy cornstarch samples were related to the fractal structures at different scale levels, with D_{m1}, D_{m2} and D_{m3} being the fractal dimensions at the lower, the intermediate, and the higher q regions respectively, while the G50 cornstarch samples just had two linear regions, with D_{m1} being the fractal dimension of the linear region at the lower q region and D_{s2} being that at the higher q region. The relationship $I \sim q^{-\alpha}$ was represented by the solid lines on the SAXS patterns in Fig. 3a and b. Based on the fractal geometry, the distinct structural features in the materials as seen at different length scales can be analyzed by the scattering patterns with multiple power-law

Table 2
SAXS parameters of native and hydrothermally treated waxy and high-amylose cornstarches.

Sample	D_{m1}/D_{s1}	D_{m2}/D_{s2}	D_{m3}/D_{s3}	q (nm^{-1})	d (nm)	I (a.u.)	Q (a.u.)	$R_{1047/1022}$
axy	2.67[a]	–	–	0.5915	10.62	3.788	0.1732 ± 0.0011	0.655
Waxy-45	2.64[a]	–	–	0.5954	10.55	3.729	0.1890 ± 0.0012	0.601
Waxy-50	2.35[a]	–	–	0.5975	10.51	3.668	0.1792 ± 0.0012	0.601
Waxy-55	2.34[a]	–	–	0.5933	10.58	3.727	0.2129 ± 0.0011	0.600
Waxy-60	2.38[a]	–	–	0.5892	10.66	3.668	0.3249 ± 0.0014	0.570
Waxy-65	2.26[a]	–	–	0.5904	10.64	2.374	0.2675 ± 0.0010	0.495
Waxy-70	1.94[a]	–	–	0.5925	10.60	1.119	0.1759 ± 0.0006	0.446
Waxy-75	2.02[a]	0.96[a]	1.42[a]	–	–	–	0.0486 ± 0.0004	0.437
Waxy-80	2.04[a]	0.97[a]	1.43[a]	–	–	–	0.0497 ± 0.0004	0.425
Waxy-85	1.63[a]	0.95[a]	1.43[a]	–	–	–	0.0558 ± 0.0004	0.430
Waxy-90	1.63[a]	0.92[a]	1.49[a]	–	–	–	0.0568 ± 0.0004	0.432
G50	2.07[b]	–	–	0.5963	10.53	1.036	0.0902 ± 0.0007	0.482
G50-45	2.73[b]	–	–	0.5987	10.49	1.219	0.0732 ± 0.0006	0.492
G50-50	2.70[b]	–	–	0.5936	10.58	1.201	0.0742 ± 0.0007	0.487
G50-55	2.85[b]	–	–	0.5960	10.54	1.201	0.0792 ± 0.0006	0.488
G50-60	2.95[a]	–	–	0.5984	10.50	1.209	0.0886 ± 0.0006	0.486
G50-65	2.71[a]	–	–	0.5984	10.50	1.333	0.1308 ± 0.0008	0.488
G50-70	2.16[a]	–	–	0.5842	10.75	1.593	0.2700 ± 0.0009	0.481
G50-75	1.39[a]	2.65[b]	–	–	–	–	0.5117 ± 0.0011	0.473
G50-80	1.15[a]	2.68[b]	–	–	–	–	0.6690 ± 0.0011	0.473
G50-85	1.06[a]	2.59[b]	–	–	–	–	0.8092 ± 0.0011	0.447
G50-90	1.00[a]	2.50[b]	–	–	–	–	0.8821 ± 0.0013	0.440

[a] Mass fractal structure.
[b] Surface fractal structure.

regions (Chavan, Sastry, & Tyagi, 2008; Emmerling & Fricke, 1992), and the upper and lower values of the size of the entities in the corresponding regions are represented by the crossovers points (or the position of intersection of the slopes) separating the power-law regions.

As seen from Fig. 3a and b and Table 2, mass fractal structures in the ranges of around 27.19 nm $< d <$ 80.00 nm, 9.78 nm $< d <$ 27.19 nm, and 5.98 nm $< d <$ 9.78 nm with respectively the fractal dimensions $D_{m1} = 1.63–2.04$, $D_{m2} = 0.92–0.97$ and $D_{m3} = 1.42–1.49$ were observed for the waxy cornstarch samples heated at the temperature equal to or higher than 75 °C. On the other hand, G50-75 was characterized by a mass fractal structure in the range of around 13.99 nm $< d <$ 80.00 nm with the fractal dimension $D_{m1} = 1.39$ and a surface fractal structure in the range of around 6.17 nm $< d <$ 13.99 nm with the fractal dimension $D_{s2} = 2.65$. However, for the G50 samples heated at temperatures higher than 75 °C, mass fractal structures in the range of around 18.31 nm $< d <$ 80.00 nm with the fractal dimension $D_{m1} = 1.00–1.15$ and surface fractal structures in the range of around 6.17 nm $< d <$ 18.31 nm with the fractal dimension $D_{s2} = 2.50–2.68$ were observed. These results show that, while the fractal aggregation type (starting from the lower scale level) remained the same for waxy cornstarch, it changed from surface fractals to mass fractals for G50 cornstarch, suggesting that the scattering objects at the lower or intermediate scale level could form a mass fractal structure at a higher scale level with different compactness (D_{m1}) depending on the temperature higher than 70 °C. As native G50 cornstarch contained more amylose than native waxy cornstarch, most of the lipid of native G50 cornstarch could be bounded with the amylose to form amylose–lipid complex which needed a higher temperature to complete its melting. Therefore, during the hydrothermal treatment at the temperature equal to or higher than 75 °C, the amylose–lipid complex could affect the formation of multifractal structures. As a result, waxy cornstarch displayed three fractal regions, whereas G50 cornstarch just showed two fractal regions. Combined with the DSC analysis, it could be also concluded that the inhomogeneity was presented at a colloidal level in the gelatinized waxy cornstarch samples, while the inhomogeneity was shown at a nano-particle (consisting of crystalline and colloidal materials) level in the G50 cornstarch samples, since multiple fractal regions were observed.

3.4. Lamellar characteristics

Six parameters of a theoretical model for the lamellar structure in starch can be obtained from the SAXS data (Cameron & Donald, 1993a, 1993b), i.e., d, the average thickness of the semi-crystalline lamellae; φ, the average thickness of the crystalline lamellae of the semi-crystalline lamellae; β, a constant, related to the widths of the Gaussian distributions of thicknesses of the semi-crystalline lamellae; N, the number of repeats of the semi-crystalline lamellae of a growth ring; $\Delta\rho = \rho_c - \rho_a$ (where ρ_c and ρ_a are the electron densities of the crystalline regions and the amorphous regions in the semi-crystalline lamellae), the difference in electron density between the crystalline lamellae and the amorphous lamellae; $\Delta\rho_u = \rho_u - \rho_a$ (where ρ_u is the electron density of the amorphous background), the difference in election density between the amorphous lamellae and the amorphous background. The value of d in starch is normally calculated using the position of the peak at around 0.6 nm^{-1} according to the Woolf-Bragg's equation $d = 2\pi/q$ (Blazek & Gilbert, 2010; Vermeylen, Goderis, & Delcour, 2006; Zhang, Chen, Liu, & Wang, 2010). Table 2 shows the SAXS parameters from the peaks of the different samples. It can be seen from Table 2 that the average thickness of the semi-crystalline lamellae (alternating crystalline and amorphous lamellae) of waxy and G50 cornstarches was 10.62 and 10.53 nm respectively, which changed slightly with the temperature increase, but disappeared when the temperature was higher than 70 °C due to the appearance of multiple fractal regions.

The log I – log q SAXS patterns of waxy and G50 cornstarches heated in abundant water are presented in Fig. 3c and d. Based on a previous study (Cameron & Donald, 1992), $\Delta\rho_u$ displays the concurrent effects of raising the low-angle intensity and lowering the definition of the peak without changing the peak position, while the major effect of increasing $\Delta\rho$ is to increase the overall intensity, including the peak intensity (I). For waxy cornstarch, as the temperature increased to 60 °C, the scattering intensity at the low q region showed a rising trend, mainly due to an increase in $\Delta\rho_u$ since

I just changed slightly but the definition of peak was lowered. One explanation for this could be that during heating in this temperature range the amorphous background absorbed more water than did the amorphous lamellae, leading to a greater difference in the election density between the amorphous lamellae and the amorphous background. In addition, compared with that for Waxy-60, dramatic decreases in *I* were seen for Waxy-65 and Waxy-70, which was mainly attributed to the smaller values of $\Delta\rho$, related to the destruction in the crystalline lamellae. However, with the temperature increasing to 60 °C, each of the hydrothermally treated G50 cornstarch samples possessed greater overall scattering intensity at the *q* region around the peak than native G50 cornstarch, indicating the hydrothermal treatment in this temperature range changed the physicochemical properties of G50 cornstarch, resulting from a relatively higher degree of the influence on the amorphous lamellae, leading to an increase in the value of $\Delta\rho$. Moreover, G50-65 and G50-70 presented a lower definition of the peak but higher intensity at the low *q* region, which should be related to both $\Delta\rho$ and $\Delta\rho_u$. To be more accurate, the hydrothermal treatment at 65 and 70 °C could lead to the greatest destruction to the amorphous background, the intermediate destruction to the amorphous lamellae, and the weakest destruction to the crystalline lamellae, contributing to the larger $\Delta\rho$ and $\Delta\rho_u$.

3.5. Mixing within phases and scattering invariant

The detailed microstructure of a polymer can be interpreted by its systematic deviation from Porod's law: $I^*q^4 - q^2$. Fig. 4 a and b show the ln $(I^*q^4) - q^2$ SAXS patterns of waxy and G50 cornstarches heated in abundant water, which could be used to analyze the deviations from Porod's law (Hashimoto, Fujimura, & Kawai, 1980). It is apparent that all the samples displayed a typical positive deviation from Porod's law at high angles, due to the presence of thermal density fluctuations or mixing within phases (Koberstein, Morra, & Stein, 1980). As shown in Fig. 4, being heated in abundant water, the waxy cornstarch samples generally showed an increasing trend on the degree of deviation from Porod's law; to be more precise, no apparent changes in the degree of deviation from Porod's law (mixing within phases between the crystalline and amorphous materials) were seen for the waxy cornstarch samples heated at temperatures lower than 60 °C, and the degree of mixing within phases increased gradually with the temperature increasing from 60 °C to 75 °C, and this degree changed slightly at even higher temperatures. However, the G50 samples had similar Porod SAXS patterns at different temperatures, indicating the mixing within phases between the crystalline and amorphous materials of G50 cornstarch changed slightly.

For a two-phase system, the scattering invariant (*Q*) is normally acquired from SAXS data by:

$$Q = 4\pi \int_0^\infty q^2 I(q) dq = V\varphi_1\varphi_2(\rho_1 - \rho_2)^2 \quad (3)$$

where *V* is the scattering volume of the sample which is a consistent value in the present study since the same X-ray source, sample cell, and same amount of sample were used; φ_1 and φ_2 are the factions of the crystalline and amorphous materials respectively; and ρ_1 and ρ_2 are the electron densities of the crystalline and amorphous materials respectively. Table 2 shows the *Q* values of waxy and G50 cornstarches heated in abundant water. It is shown that as the temperature rose, the *Q* of waxy cornstarch first increased and then decreased, but the *Q* of G50 cornstarch displayed a consistent increasing trend. With the temperature increasing up to 60 °C, no obvious change in the crystalline structure of waxy cornstarch was seen (see the WAXD analysis shown later), but an increasing amount of water was absorbed into the amorphous material. As a result, while the product value of $\varphi_1{}^*\varphi_2$ changed slightly, the value of $(\rho_1 - \rho_2)^2$ became larger, leading to a rising value of *Q*. Furthermore, with the hydrothermal treatment at temperatures higher than 60 °C, the crystalline structure of waxy cornstarch was gradually destroyed and the granules became larger, thus the values of $\varphi_1{}^*\varphi_2$ (to the best of our knowledge, $\varphi_1 < 0.5$), and $(\rho_1 - \rho_2)^2$ became smaller, contributing to a smaller *Q*. However, the *Q* of G50 cornstarch increased with the temperature increase, which was attributed to relatively greater destruction to the amorphous material. In other words, compared with the crystalline material, a larger amount of water entered into the

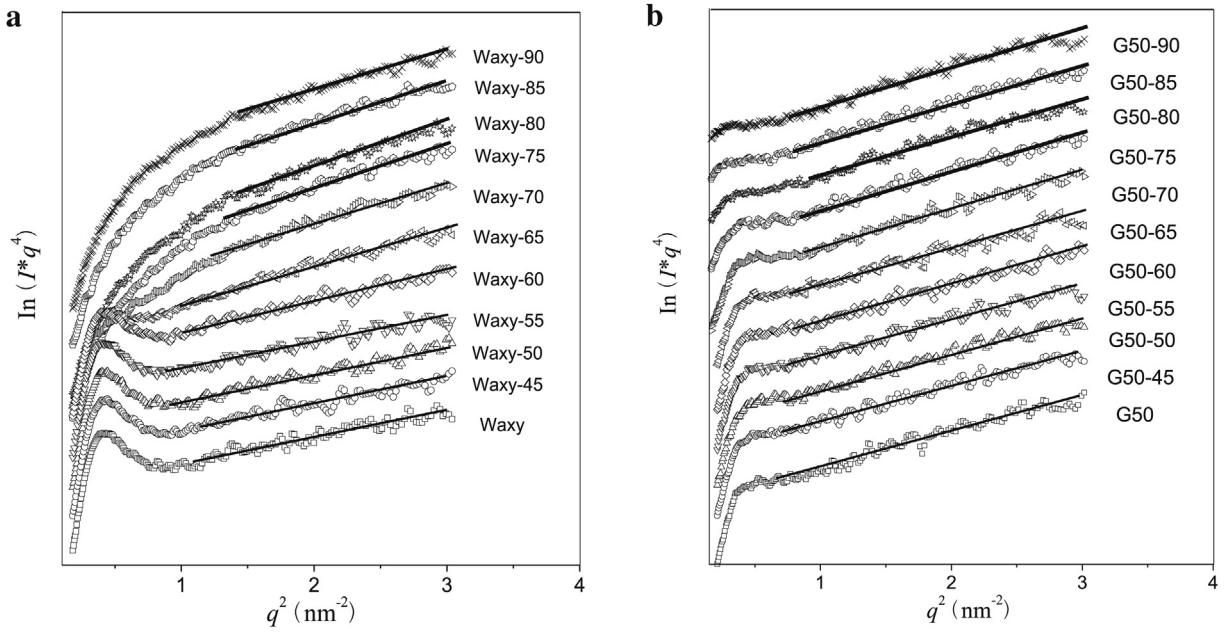

Fig. 4. Porod SAXS patterns of native and hydrothermally treated waxy and high-amylose cornstarches (waxy (a), G50 (d)).

amorphous material of G50 cornstarch during being heated in abundant water, leading to a larger value of Q, related to both an increase in the value of $(\rho_1 - \rho_2)^2$ and a gradually decrease in the value of $\varphi_1{}^*\varphi_2$.

3.6. Crystalline characteristics

Normally, a polarization cross (birefringence) can be observed when the starch granule is exposed under polarized light because of the anisotropic phenomenon, attributed to the orderly arranged starch molecules of the crystalline regions and the disorderly arranged starch molecules of the amorphous regions in the starch granule (Zhang, Chen, et al., 2013; Zhang, Li, et al., 2013). The intensity of birefringence is related to the granular size, degree of crystallinity, and microcrystalline orientation. The polarized light microscopic images of waxy and G50 cornstarches heated in abundant water at different temperatures are shown in Fig. 2. It is noted that native waxy cornstarch showed greater birefringence intensity than native G50 cornstarch. For waxy cornstarch, the birefringence intensity remained almost the same by the temperature 60 °C and then decreased slightly at 65 °C before a dramatic reduction in the range between 65 °C and 70 °C, and no polarization crosses were seen when the temperature reached 75 °C which was lower than the T_c of endotherm G. This implies that the anisotropy of waxy cornstarch experienced a sharp decrease at the initial period of gelatinization (65 °C–70 °C) and disappeared before the end of gelatinization. However, for G50 cornstarch, no apparent change in the birefringence intensity was observed before 70 °C, and this intensity then fell gradually with the increased temperature but some polarization crosses could be even seen for G50-90. These results were expected since G50 cornstarch possessed a broader temperature range of gelatinization (see the DSC analysis).

Depending on the packing of the amylopectin side chains into double-helices or the amylose single helices, the starch crystalline structure can be described as either A, B, C, or V (Buleon et al., 1998; Gernat et al., 1990; Luengwilai & Beckles, 2009; Sarko & Wu, 1978). For a specific type of starch, a certain WAXD pattern can be obtained due to the fact that the starch granule is a semi-crystalline system, consisting of crystalline and amorphous regions, and the WAXD patterns of the crystalline parts of starch always have sharp peaks, while those of the amorphous parts of starch are dispersive (Gernat et al., 1990). Fig. 5 a and b show the WAXD patterns of waxy and G50 cornstarches heated in abundant water at different temperatures. It is seen that native waxy cornstarch displayed a typical A-type crystalline structure with main diffraction peaks at round 15, 17, 18 and 23° (2θ), whereas native G50 cornstarch had a typical B-type crystalline structure with main diffraction peaks at round 17, 22 and 24° (2θ) and a V-type crystalline structure with a peak at round 19.8° (2θ) which was a typical amylose–lipid complex diffraction peak (Buleon et al., 1998), suggesting a B + V type hybrid polymorph. The A-type crystalline structure of waxy cornstarch was destroyed significantly at 65 °C, less obvious characteristics could be seen after being heated at 70 °C, and no peaks were observed at even higher temperatures. However, the peak intensities of the B-type crystalline structure of G50 cornstarch fell gradually with increasing the temperature up to 90 °C. It is worth noting that the peak of V-type crystalline structure at round 19.8° (2θ) just changed slightly even when the temperature reached 90 °C, indicating the requirement of an even higher temperature for the melting of amylose–lipid complex. These results were reasonable since G50 cornstarch possessed much more amylose, forming a higher amount of amylose–lipid complex crystals (V-type crystals) which need a temperature higher than 107 °C to complete the melting process in excess water (see DSC analysis).

The infrared (IR) spectrum in the region of 800–1200 cm^{-1} has been widely applied to analyze the crystalline structure of starch (Sevenou, Hill, Farhat, & Mitchell, 2002; van Soest, Tournois, de Wit, & Vliegenthart, 1995). The IR absorbance band at 1047 cm^{-1} is sensitive to the crystalline structure; and the band at 1022 cm^{-1} has a relationship with the amorphous structure. Hence, the ratio of intensity at 1047/1022 cm^{-1} ($R_{1047/1022}$) can be used to analyze the changes in the crystalline structure (van Soest et al., 1995). Table 2 shows the values of $R_{1047/1022}$ for the native and hydrothermally treated cornstarches with abundant water. As the temperature increased, the $R_{1047/1022}$ of waxy cornstarch fell more significantly than that of G50 cornstarch, indicating the crystalline structure of waxy cornstarch was more susceptible to the hydrothermal treatment, which in good agreement with those results from above analyses.

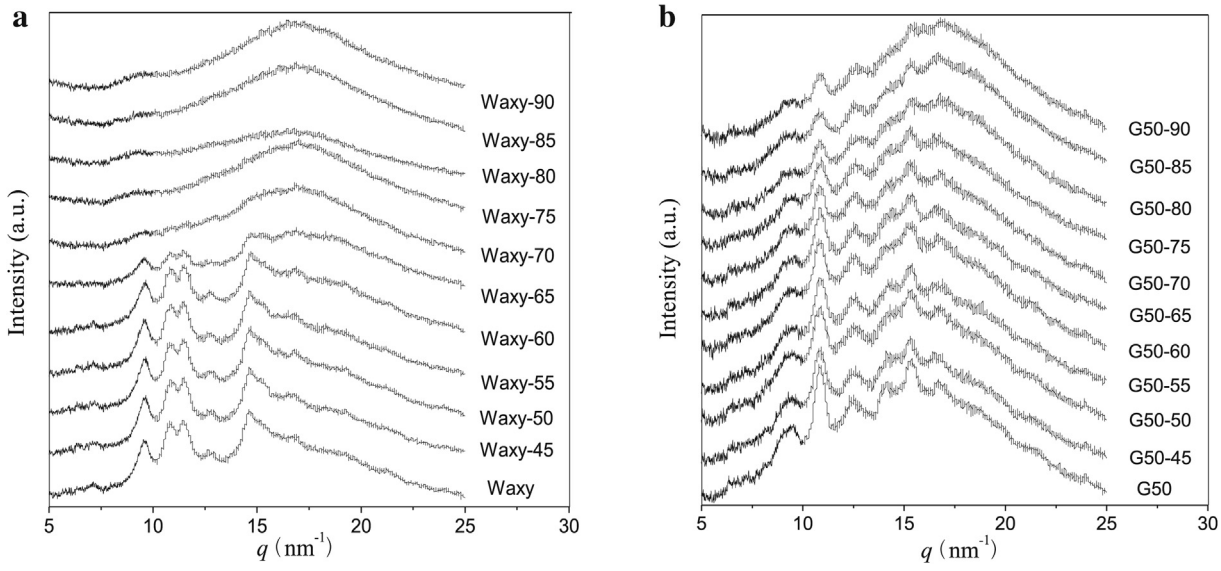

Fig. 5. WAXD patterns of native and hydrothermally treated waxy and high-amylose cornstarches (waxy (a) and G50 (b)).

4. Conclusion

In the present work, it was found that native waxy cornstarch displayed only one endotherm (G) in excess water, while there were two endotherms (G and M2) for native G50 cornstarch. During heating in abundant water, waxy cornstarch granules could swell dramatically at around the T_o of endotherm G and even break at 75 °C which was lower than the T_c, while G50 cornstarch granules presented a less significant increase in the volume near the T_o of endotherm G and no granules disappeared during the melting of amylopectin. This is because of that the amylose–lipid complex needed a higher temperature to complete its melting, thus the granules of G50 cornstarch were more difficult to swell and even to break during the hydrothermal treatment. As the temperature increased to 70 °C, the scattering objects in both waxy and G50 cornstarches became looser.

Interestingly, when the temperature was equal to or higher than 75 °C which was near the T_c of endotherm G of waxy cornstarch, mass fractal structures in the waxy cornstarch samples at different scale levels were formed, suggesting the inhomogeneity at a nano-colloidal level in these samples. Nevertheless, the temperature equal to or higher than 75 °C which was near the T_o of endotherm G of G50 cornstarch led to the formation of a mass fractal structure at the higher scale level and a surface fractal structure at the lower scale level for G50 cornstarch samples. This suggests the inhomogeneity at a nanoparticle level in these G50 cornstarch samples. For these two cornstarches, the scattering objects at the lower or intermediate scale level could form a mass fractal structure at a higher scale level with different compactness (D_{m1}) depending on the temperature ($\geq$75 °C) used.

Furthermore, the average thickness of the semi-crystalline lamellae of waxy and G50 cornstarches changed slightly with an initial increase in the temperature, but disappeared when the samples were hydrothermally treated at a temperature of 75 °C or higher, due to the existence of multiple fractal structures. It was noted that in the temperature range of 45–60 °C, the amorphous background in waxy cornstarch absorbed more water than did the amorphous lamellae, leading to a larger $\Delta\rho_u$, while the amorphous lamellae in G50 cornstarch received a greater influence than the crystalline lamellae, resulting in an increase in the value of $\Delta\rho$. Waxy-65 and Waxy-70 experienced dramatic destruction to their crystalline lamellae; however, G50-65 and G50-70 had the greatest destruction to the amorphous background, the intermediate destruction to the amorphous lamellae, and the weakest destruction to the crystalline lamellae.

Additionally, the anisotropy and A-type crystalline structure of waxy cornstarch displayed a sharp decrease at the initial stage of gelatinization and disappeared before the end of gelatinization. For G50 cornstarch, no obvious changes in the birefringence and the WAXD peak intensities (B-type crystalline structure) were observed when the temperature was lower than the T_o of endotherm G, and these intensities fell gradually with a further increase in the temperature. Interestingly, the peak of V-type crystalline structure at round 19.8° (2θ) just experienced a minor change even when the temperature was increased up to 90 °C, indicating the requirement of an even higher temperature for the melting of amylose–lipid complex.

These results are important for further investigations on the supramolecular structural changes of cornstarches with different amylose/amylopectin ratios during being processed with abundant water. Fundamental data are presented here for further studies on the relationships between supramolecular structures and properties of cornstarch to widen the application of cornstarch in foods.

Acknowledgments

The authors would like to acknowledge the National Natural Science Funds of China (No. 31071503, 31130042), the National Science and Technology Supporting Program Projects (2012BAD34B07), the Special R&D Funds for the Doctoral Discipline Stations in Universities, Ministry of Education (20120172110014) and the Office of Education of Guangdong Province Science and Technology Innovation (Key) Projects in Universities (2012CXZD0006)

References

Atwell, W. A., Hood, L. F., Lineback, D. R., Varriano-Marston, E., & Zobel, H. F. (1988). The terminology and methodology associated with basic starch phenomena. *Cereal Food Worlds, 33*, 306–311.

Bastos, D. C., Santos, A. E. F., da Silva, M. L. V. J., & Simao, R. A. (2009). Hydrophobic corn starch thermoplastic films produced by plasma treatment. *Ultramicroscopy, 109*, 1089–1093.

Blazek, J., & Gilbert, E. P. (2010). Effect of enzymatic hydrolysis on native starch granule structure. *Biomacromolecules, 11*, 3275–3289.

Buleon, A., Colonna, P., Planchot, V., & Ball, S. (1998). Starch granules: structure and biosynthesis. *International Journal of Biological Macromolecules, 23*, 85–112.

Cameron, R. E., & Donald, A. M. (1992). A small-angle X-ray scattering study of the annealing and gelatinization of starch. *Polymer, 33*(12), 2628–2635.

Cameron, R. E., & Donald, A. M. (1993a). A small-angle X-ray scattering study of the absorption of water into the starch granule. *Carbohydrate Research, 244*, 225–236.

Cameron, R. E., & Donald, A. M. (1993b). A small-angle X-ray scattering study of starch gelatinization in excess and limiting water. *Journal of Polymer Science: Part B: Polymer Physics, 31*, 1197–1203.

Chang, F. D., He, X. W., & Huang, Q. (2013). Effect of lauric acid on the V-amylose complex distribution and properties of swelled normal cornstarch granules. *Journal of Cereal Science, 58*, 89–95.

Chavan, S. V., Sastry, P. U., & Tyagi, A. K. (2008). Fractal and agglomeration behavior in Gd and Sm doped CeO2 nano-crystalline powders. *Journal of Alloys and Compounds, 457*, 440–446.

Emmerling, A., & Fricke, J. (1992). Small angle scattering and the structure of aerogels. *Journal of Non-Crystalline Solids, 145*, 113–120.

Gernat, C., Tadosta, S., & Damaschun, G. (1990). Supramolecular structure of legume starches revealed by X-ray scattering. *Starch/Stärke, 42*(5), 175–178.

Hashimoto, T., Fujimura, M., & Kawai, H. (1980). Domain-boundary structure of styrene-isoprene block copolymer films cast from solutions. 5. Molecular-weight dependence of spherical microdomains. *Macromolecules, 13*, 1660–1669.

Jiang, Q. Q., Gao, W. Y., Li, X., & Zhang, J. Z. (2011). Characteristics of native and enzymatically hydrolyzed *Zea mays* L., *Fritillaria, ussuriensis* Maxim. and *Dioscorea opposita* Thunb. Starches. *Food Hydrocolloids, 25*, 521–528.

Juansang, J., Puttanlek, C., Rungsardthong, V., Puncha-arnon, S., & Uttapap, D. (2012). Effect of gelatinisation on slowly digestible starch and resistant starch of heat-moisture treated and chemically modified canna starches. *Food Chemistry, 131*, 500–507.

Karim, A. A., Norziah, M. H., & Seow, C. C. (2000). Methods for the study of starch retrogradation. *Food Chemistry, 71*, 9–36.

Kim, K. S., & Huber, K. C. (2010). Physicochemical properties and amylopectin fine structures of A- and B-type granules of waxy and normal soft wheat starch. *Journal of Cereal Science, 51*, 256–264.

Koberstein, J. T., Morra, B., & Stein, R. S. (1980). Determination of diffuse-boundary thicknesses of polymers by small-angle X-ray scattering. *Journal of Applied Crystallography, 13*, 34–45.

Liu, W. C., Halley, P. J., & Gilbert, R. G. (2010). Mechanism of degradation of starch, a highly branched polymer, during extrusion. *Macromolecules, 43*, 2855–2864.

Liu, H. S., Yu, L., Xie, F. W., & Chen, L. (2006). Gelatinization of corn starch with different amylose/amylopectin content. *Carbohydrate Polymers, 65*(3), 357–363.

Luengwilai, K., & Beckles, D. M. (2009). Structural investigations and morphology of tomato fruit starch. *Journal of Agricultural and Food Chemistry, 57*, 282–291.

Nara, S., & Komiya, T. (1983). Studies on the relationship between water-saturated state and crystallinity by the diffraction method for moistened potato starch. *Starch/Stärke, 35*, 407–410.

Oates, C. G. (1997). Towards an understanding of starch granule structure and hydrolysis. *Trends in Food Science & Technology, 8*, 375–382.

Pikus, S. (2005). Small angle X-ray scattering (SAXS) studies the structure of starch and starch products. *Bio-polymers and Conducting Polymers, 13*(5), 82–86.

Sarko, A., & Wu, H. C. (1978). The crystal structures of A-, B-, and C-polymorphs of amylose and starch. *Starch/Stärke, 30*, 73–78.

Sevenou, O., Hill, S. E., Farhat, I. A., & Mitchell, J. R. (2002). Organisation of the external region of the starch granule as determined by infrared spectroscopy. *International Journal of Biological Macromolecules, 31*, 79–85.

Suzuki, T., Chiha, A., & Yano, T. (1997). Interpretation of small angle X-ray scattering from starch on the basis of fractals. *Carbohydrate Polymers, 34*, 357–363.

van Soest, J. J. G., Tournois, H., de Wit, D., & Vliegenthart, J. F. G. (1995). Short-range structure in (partially) crystalline potato starch determined with attenuated total reflectance Fourier-transform IR spectroscopy. *Carbohydrate Research, 279*, 201–214.

Vermeylen, R., Goderis, B., & Delcour, J. A. (2006). An X-ray study of hydrothermally treated potato starch. *Carbohydrate Polymers, 64*, 364–375.
Wang, X. Y., Chen, L., Li, X. X., Xie, F. W., Liu, H. S., & Yu, L. (2011). Thermal and rheological properties of breadfruit starch. *Journal of Food Science, 76*(1), E56–E61.
Yu, L., & Christie, G. (2001). Measurement of starch thermal transitions using differential scanning calorimetry. *Carbohydrate Polymers, 46*(2), 179–184.
Zhang, J., Chen, F., Liu, F., & Wang, Z. W. (2010). Study on structural changes of microwave heat-moisture treated resistant *Canna edulis* Ker starch during digestion in vitro. *Food Hydrocolloids, 24*, 27–34.
Zhang, B. J., Chen, L., Zhao, Y., & Li, X. X. (2013). Structure and enzymatic resistivity of debranched high temperature-pressure treated high-amylose corn starch. *Journal of Cereal Science, 57*, 348–355.
Zhang, B. J., Li, X. X., Liu, J., Xie, F. W., & Chen, L. (2013). Supramolecular structure of A- and B-type granules of wheat starch. *Food Hydrocolloids, 31*, 68–73.
Zhu, J., Li, L., Chen, L., & Li, X. X. (2012). Study on supramolecular structural changes of ultrasonic treated potato starch granules. *Food Hydrocolloids, 29*, 116–122.
Zobel, H. F. (1988). Molecules to granules: a comprehensive starch review. *Starch/Starke, 40*(2), 44–50.